gradually replace $Na_v1.2$ in a population of excitatory neurons during maturation.[16,17] In fact, the developmental shift in splicing of *SCN8A* exon 18 to a transcript encoding the full length protein is still incomplete at 10 months of age.[7] Therefore, it can be postulated that the onset of seizures may be earlier in cases with *SCN2A* mutations compared with *SCN8A* mutations. Our present study supports this hypothesis, as only 2 (28.6%) of 7 cases with *SCN8A* mutations had an onset during the neonatal period, whereas 11 (73.3%) of 15 cases with *SCN2A* mutations previously showed a neonatal seizure onset.[18]

Regarding the functional properties of each domain, at least three types of aberrations appear to be involved: voltage sensing, inactivation, and the interaction of accessory proteins. Two mutations (p.Phe846Ser and p.Arg1617Gln) were located in S4 transmembrane segments, which play a key role in voltage sensing and undergo a conformational change when the pore opens.[1,16] Therefore, these mutations may alter both the activation and inactivation of $Na_v1.6$ consistent with the demonstrated effect on activation of the *SCN8A* mutation Asn1768Asp in domain 4 transmembrane segment 6.[9] Three regions involved in inactivation contained mutations in the present study: the linker between domains III and IV that forms an inactivation gate (p.Asn1466Lys and p.Asn1466Thr),[16,19] the loop between S4 and S5 in domain IV (pAla1650Thr) that forms the inactivation gate receptor together with S6 in domain IV, and the loops between S4 and S5 in domain III (p.Ile1327-Val).[13,19] It is likely that these mutations disturb the inactivation of $Na_v1.6$. One mutation (p.Arg1872Trp) was located in the C-terminal cytoplasmic domain, which is involved in the interaction with accessory proteins such as β-subunits, calmodulin, G protein, and the antiepileptic drug phenytoin.[16,20,21] This mutation is likely to affect the interaction between $Na_v1.6$ and accessory proteins.

Although we attempted to find phenotype–genotype correlations of *SCN8A* mutations based on these functional classifications, no clear correlations could be found. For example, mutations in patients 1 and 5 were located in the same codon (Asn1466) involving channel inactivation, but the onset and type of seizures differed between the two patients (3 days and 4 months). Similarly, patients 3 and 4 both had mutations in the S4 domain, but their clinical courses were quite different. Further study of functional characterization of the effects of de novo mutations on *SCN8A* activity may reveal relationships to clinical course and drug response. Furthermore, a lack of clear phenotype–genotype correlations may suggest the involvement of genetic modifiers. In fact, examples of interactions between channel variants have been described previously; the *Scn8a*$^{med\text{-}jo/+}$ mutation can rescue the seizures and premature lethality of *Scn1a*$^{+/-}$ mice, demonstrating the existence of genetic interactions between *Scn1a* and *Scn8a*.[22] In humans, it has been suggested that *SCN9A* is a modifier of *SCN1A*-related epilepsies such as genetic epilepsy with febrile seizure plus and Dravet syndrome.[23,24] Next-generation sequencing has enabled the comprehensive examination of mutations and should provide information about candidate modifier genes.

A nonsense *SCN8A* mutation was reported previously in a patient with intellectual disability, pancerebellar atrophy, and cerebellar ataxia, but without epilepsy.[25] Moreover, mice carrying a homozygous missense mutation in *Scn8a* showed chronic ataxia with an unsteady, wide-based gait,[8,26] supporting the association between *SCN8A* mutations and cerebellar atrophy in humans. In this study, only patient 3 showed cerebellar atrophy. Analysis of a larger group of patients with *SCN8A* mutations is required to validate this issue. One interesting phenotype of *SCN8A* mutations is atypical absence seizures, as seen in patient 2. It was also reported that *Scn8a* heterozygous null mutant mice exhibit spike-wave discharges on their EEG and absence epilepsy.[27] Thus, *SCN8A* might be an important gene for human absence seizures. All the *SCN8A* mutations found in epileptic encephalopathy are missense mutations, which is in striking contrast to the predominance of loss-of-function mutations of *SCN1A* in Dravet syndrome,[28] suggesting that haploinsufficiency is not causal in the case of *SCN8A*, but rather, gain of abnormal function is likely to be involved.

Although five of the patients with an *SCN8A* mutation showed severe developmental delay, two patients showed normal initial development. They showed developmental regression after seizure onset. Of interest, they regained some developmental improvement upon seizure control. This fact indicates that in some patients with a *SCN8A* mutation, control of seizure may ameliorate development.

Dravet syndrome, which is caused by *SCN1A* mutations, shows one of the highest rates of sudden death in patients with epilepsy, ranging from 5.7% to 10% in studied cohorts, and the rate is estimated at about 30-fold higher than in patients with other pediatric-onset epilepsies.[29] Veeramah et al.[9] reported that a patient with a de novo *SCN8A* mutation died from SUDEP at the age of 15 years. Patients in this study are all younger than this and SUDEP is rare in children with epilepsy before the age of 15.[30] However, tonic–clonic seizures, treatment-resistant epilepsy, developmental delay, and neurologic disorders such as intellectual disability and cerebral palsy are all risk factors for SUDEP[30]; most of these risk factors are present in our patients. We suggest that careful follow-up is warranted in patients with *SCN8A* mutations to monitor the potential development of SUDEP.

Acknowledgments

We would like to thank all patients and their families for their participation in this study. We also thank Nobuko Watanabe for her technical assistance. Supported by the Ministry of Health, Labour and Welfare of Japan; the Japan Society for the Promotion of Science (a Grant-in-Aid for Scientific Research [B] from [25293085, 25293235], a Grant-in-Aid for Scientific Research [A] [13313587], a Grant-in-Aid for Scientific Research [C] [24591500]); the Takeda Science Foundation; the Japan Science and

Technology Agency; the Strategic Research Program for Brain Sciences (11105137); and a Grant-in-Aid for Scientific Research on Innovative Areas (Transcription Cycle) from the Ministry of Education, Culture, Sports, Science and Technology of Japan (12024421).

Conflict of Interest

We confirm that we have read the Journal's position on issues involved in ethical publication and affirm that this report is consistent with those guidelines. None of the authors has any conflict of interest to disclose.

References

1. Lai HC, Jan LY. The distribution and targeting of neuronal voltage-gated ion channels. *Nat Rev Neurosci* 2006;7:548–562.
2. Oliva M, Berkovic SF, Petrou S. Sodium channels and the neurobiology of epilepsy. *Epilepsia* 2012;53:1849–1859.
3. Meisler MH, Kearney JA. Sodium channel mutations in epilepsy and other neurological disorders. *J Clin Invest* 2005;115:2010–2017.
4. Whitaker WR, Faull RL, Waldvogel HJ, et al. Comparative distribution of voltage-gated sodium channel proteins in human brain. *Brain Res Mol Brain Res* 2001;88:37–53.
5. Meisler MH, O'Brien JE, Sharkey LM. Sodium channel gene family: epilepsy mutations, gene interactions and modifier effects. *J Physiol* 2010;588:1841–1848.
6. Caldwell JH, Schaller KL, Lasher RS, et al. Sodium channel Na(v)1.6 is localized at nodes of ranvier, dendrites, and synapses. *Proc Natl Acad Sci USA* 2000;97:5616–5620.
7. O'Brien JE, Drews VL, Jones JM, et al. Rbfox proteins regulate alternative splicing of neuronal sodium channel *SCN8A*. *Mol Cell Neurosci* 2012;49:120–126.
8. O'Brien JE, Meisler MH. Sodium channel *SCN8A* (Nav1.6): properties and *de novo* mutations in epileptic encephalopathy and intellectual disability. *Front Genet* 2013;4:213.
9. Veeramah KR, O'Brien JE, Meisler MH, et al. De novo pathogenic *SCN8A* mutation identified by whole-genome sequencing of a family quartet affected by infantile epileptic encephalopathy and SUDEP. *Am J Hum Genet* 2012;90:502–510.
10. Allen AS, Berkovic SF, Cossette P, et al. *De novo* mutations in epileptic encephalopathies. *Nature* 2013;501:217–221.
11. Carvill GL, Heavin SB, Yendle SC, et al. Targeted resequencing in epileptic encephalopathies identifies *de novo* mutations in *CHD2* and *SYNGAP1*. *Nat Genet* 2013;45:825–830.
12. Rauch A, Wieczorek D, Graf E, et al. Range of genetic mutations associated with severe non-syndromic sporadic intellectual disability: an exome sequencing study. *Lancet* 2012;380:1674–1682.
13. Vaher U, Noukas M, Nikopensius T, et al. *De novo SCN8A* mutation identified by whole-exome sequencing in a boy with neonatal epileptic encephalopathy, multiple congenital anomalies, and movement disorders. *J Child Neurol* 2013; Dec 18 [Epub ahead of print].
14. Kodera H, Kato M, Nord AS, et al. Targeted capture and sequencing for detection of mutations causing early onset epileptic encephalopathy. *Epilepsia* 2013;54:1262–1269.
15. Saitsu H, Nishimura T, Muramatsu K, et al. *De novo* mutations in the autophagy gene *WDR45* cause static encephalopathy of childhood with neurodegeneration in adulthood. *Nat Genet* 2013;45:445–449, 9e1.
16. Eijkelkamp N, Linley JE, Baker MD, et al. Neurological perspectives on voltage-gated sodium channels. *Brain* 2012;135:2585–2612.
17. Liao Y, Deprez L, Maljevic S, et al. Molecular correlates of age-dependent seizures in an inherited neonatal-infantile epilepsy. *Brain* 2010;133:1403–1414.
18. Nakamura K, Kato M, Osaka H, et al. Clinical spectrum of *SCN2A* mutations expanding to Ohtahara syndrome. *Neurology* 2013;81:992–998.
19. Catterall WA. From ionic currents to molecular mechanisms: the structure and function of voltage-gated sodium channels. *Neuron* 2000;26:13–25.
20. Rusconi R, Scalmani P, Cassulini RR, et al. Modulatory proteins can rescue a trafficking defective epileptogenic Nav1.1 Na+ channel mutant. *J Neurosci* 2007;27:11037–11046.
21. Vacher H, Trimmer JS. Trafficking mechanisms underlying neuronal voltage-gated ion channel localization at the axon initial segment. *Epilepsia* 2012;53(Suppl. 9):21–31.
22. Martin MS, Tang B, Papale LA, et al. The voltage-gated sodium channel *Scn8a* is a genetic modifier of severe myoclonic epilepsy of infancy. *Hum Mol Genet* 2007;16:2892–2899.
23. Singh NA, Pappas C, Dahle EJ, et al. A role of *SCN9A* in human epilepsies, as a cause of febrile seizures and as a potential modifier of Dravet syndrome. *PLoS Genet* 2009;5:e1000649.
24. Mulley JC, Hodgson B, McMahon JM, et al. Role of the sodium channel *SCN9A* in genetic epilepsy with febrile seizures plus and Dravet syndrome. *Epilepsia* 2013;54:e122–e126.
25. Trudeau MM, Dalton JC, Day JW, et al. Heterozygosity for a protein truncation mutation of sodium channel *SCN8A* in a patient with cerebellar atrophy, ataxia, and mental retardation. *J Med Genet* 2006;43:527–530.
26. Meisler MH, Plummer NW, Burgess DL, et al. Allelic mutations of the sodium channel SCN8A reveal multiple cellular and physiological functions. *Genetica* 2004;122:37–45.
27. Papale LA, Beyer B, Jones JM, et al. Heterozygous mutations of the voltage-gated sodium channel *SCN8A* are associated with spike-wave discharges and absence epilepsy in mice. *Hum Mol Genet* 2009;18:1633–1641.
28. Escayg A, Goldin AL. Sodium channel *SCN1A* and epilepsy: mutations and mechanisms. *Epilepsia* 2010;51:1650–1658.
29. Kalume F. Sudden unexpected death in Dravet syndrome: respiratory and other physiological dysfunctions. *Respir Physiol Neurobiol* 2013;189:324–328.
30. Devinsky O. Sudden, unexpected death in epilepsy. *N Engl J Med* 2011;365:1801–1811.

Supporting Information

Additional Supporting Information may be found in the online version of this article:

Appendix S1. Case reports.

Table S1. Prediction of Mutation Pathogenicity.

Figure S1. Conservation of substituted amino acids by *SCN8A* mutations.

Journal of Human Genetics (2014) 59, 691–693

www.nature.com/jhg

SHORT COMMUNICATION

The somatic *GNAQ* mutation c.548G>A (p.R183Q) is consistently found in Sturge–Weber syndrome

Mitsuko Nakashima[1], Masakazu Miyajima[2], Hidenori Sugano[2], Yasushi Iimura[2], Mitsuhiro Kato[3], Yoshinori Tsurusaki[1], Noriko Miyake[1], Hirotomo Saitsu[1], Hajime Arai[2] and Naomichi Matsumoto[1]

Sturge–Weber syndrome (SWS) is a neurocutaneous disorder characterized by capillary malformation (port-wine stains), and choroidal and leptomeningeal vascular malformations. Previously, the recurrent somatic mutation c.548G>A (p.R183Q) in the G-α q gene (*GNAQ*) was identified as causative in SWS and non-syndromic port-wine stain patients using whole-genome sequencing. In this study, we investigated somatic mutations in *GNAQ* by next-generation sequencing. We first performed targeted amplicon sequencing of 15 blood–brain-paired samples in sporadic SWS and identified the recurrent somatic c.548G>A mutation in 80% of patients (12 of 15). The percentage of mutant alleles in brain tissues of these 12 patients ranged from 3.6 to 8.9%. We found no other somatic mutations in any of the seven *GNAQ* exons in the remaining three patients without c.548G>A. These findings suggest that the recurrent somatic *GNAQ* mutation c.548G>A is the major determinant genetic factor for SWS and imply that other mutated candidate gene(s) may exist in SWS.
Journal of Human Genetics (2014) **59**, 691–693; doi:10.1038/jhg.2014.95; published online 6 November 2014

Sturge–Weber syndrome (SWS; MIM no. 185300) is a rare neurocutaneous disorder characterized by facial cutaneous vascular malformations (port-wine stains), and ocular and cerebral vascular malformations result in neurological impairment including seizures and intellectual disability.[1,2] The prevalence is estimated at ~ 1/20 000–50 000.[2] Because the occurrence of SWS is sporadic with no heritability, it is thought to be caused by somatic mutations.[3] Previously, a somatic mutation in the gene encoding the q class of guanine nucleotide-binding protein (G-protein)-α subunit (guanine nucleotide-binding protein, Q polypeptide; *GNAQ*) was identified in both SWS patients and those with non-syndromic port-wine stains.[4] Here, we investigated the presence of somatic *GNAQ* mutations in 15 SWS patients using targeted next-generation sequencing.

PATIENTS AND METHODS

Study population

A total of 15 SWS patients were recruited for this study, and complete paired sets of peripheral blood leukocytes and surgically resected brain tissues were obtained from all patients. Patients were diagnosed as having SWS if they had two or more of the following symptoms: (1) craniofacial vascular malformation, (2) early-onset seizure, (3) contralateral hemiplegia or ateliosis, (4) intellectual disability and (5) ocular findings including choroidal vascular malformations, glaucoma, buphthalmia and hemianopia. All of the individuals underwent preoperative neuroimaging with magnetic resonance imaging. Detailed clinical features are shown in Table 1. All the brain specimens were histopathologically examined and confirmed as truly leptomengial angioma. Experimental protocols were approved by the Institutional Review Board of Yokohama City University School of Medicine and Juntendo University Graduate School of Medicine. Written informed consent was obtained from patients or parents of pediatric patients.

Deep sequencing of *GNAQ* c.548G>A

Genomic DNA of RNAlater (ThermoFisher Scientific, Waltham, MA, USA)-treated brain tissue blocks and peripheral blood leukocytes was extracted using Puregene Core Kit A (Qiagen, Valencia, CA, USA) and PAXgene Blood DNA kit (Qiagen), respectively, according to the manufacturer's instruction. With genomic DNA obtained from leukocytes and tissues, the 173-bp target region including c.548G>A in *GNAQ* exon 4 was PCR-amplified using the following primers: forward 5′-ATTGTGTCTTCCCTCCTCTA-3′ and reverse 5′-GGTTT CATGGACTCAGTTAC-3′. A single-indexed sequencing library was prepared using the SureSelect XT Library Prep Kit (Agilent Technologies, Santa Clara, CA, USA) and sequenced on an Illumina HiSeq 2500 (Illumina, San Diego, CA, USA) with 101-bp paired-end reads. Image analysis and base calling were performed by sequence control software real-time analysis and CASAVA software v1.8.2 (Illumina). Quality-filtered reads were mapped to the human reference genome sequence (UCSC hg19, NCBI build 37) and aligned using Novoalign (Novocraft Technologies, Jaya, Malaysia). The aligned read files in the BAM format were sorted and indexed using SAMtools.[5] Data analysis including allele counting was performed by Integrative Genomics Viewer software.[6,7] We defined the 1% cutoff line for the presence of mutant alleles out of total reads based on the Shirley's criteria.[4]

GNAQ mutation screening

In the remaining subjects without c.548G>A, *GNAQ* mutation screening was performed using additional brain tissues. Primers were designed for the entire

[1]Department of Human Genetics, Yokohama City University Graduate School of Medicine, Yokohama, Japan; [2]Department of Neurosurgery, Juntendo University Graduate School of Medicine, Tokyo, Japan and [3]Department of Pediatrics, Yamagata University Faculty of Medicine, Yamagata, Japan
Correspondence: Dr N Matsumoto, Department of Human Genetics, Yokohama City University Graduate School of Medicine, 3-9 Fukuura, Kanazawa-ku, Yokohama 236-0004, Japan.
E-mail: naomat@yokohama-cu.ac.jp
Received 3 July 2014; revised 13 September 2014; accepted 10 October 2014; published online 6 November 2014

Table 1 Clinical features of SWS individuals and deep-sequencing results of c.548G>A in *GNAQ*

				LAs		*Seizures*				*c.548G>A mutation*		
Patients	*Sex*	*Age*	*PWS*	*Region*	*Size*	*Onset age*	*Type*	*ID*	*GL*	*Read depth (brain/blood)*	*Mutant allele frequency (%)[a] (brain/blood)*	*Assessed brain samples*
1	M	6	Face	Left	Hemisphere	3 Mon	CP	+	+	289 312/2 676 243	5.69/0.03	1
2	M	7	Face	Left	T, P, O	11 Mon	CP	+	+	1 170 532/591 208	4.03/0.05	1
3	Fe	6	Face	Right	Hemisphere	8 Mon	Pa	+	–	566 890/1 128 199	0.03–0.06/0.03	2
4	M	4	Face	Right	Hemisphere	4 Mon	Pa	+	–	996 691/1 556 151	0.16–0.28/0.03	2
5	M	5	Face	Right	T, P, O	8 Mon	Pa	–	+	490 977/471 499	5.04/0.04	1
6	M	10	Face	Right	T, O	12 Mon	CP	+	+	930 173/409 196	6.14/0.04	1
7	M	4	Face	Left	Hemisphere	4 Mon	Pa	+	+	639 834/635 419	4.11/0.04	1
8	M	3	Face	Right	Hemisphere	7 Mon	Pa	–	+	253 920/230 876	6.17/0.44	1
9	M	3	Face	Left	F, P	5 Mon	CP	–	–	1 277 805/1 128 803	7.59/0.03	1
10	M	3	Face	Left	Hemisphere	3 Mon	Pa	+	+	622 186/1 128 803	8.06/0.01	1
11	Fe	3	Head	Left	Hemisphere	2 Mon	Pa	–	–	387 543/432 693	0.03–0.04/0.03	2
12	F	2	Face	Right	Hemisphere	1 Mon	Pa	–	–	65 437/20 297	3.77/0.04	1
13	M	7	Face	Right	F	4 Years	CP	+	–	611 093/441 137	3.91/0.03	1
14	Fe	2	—	Right	Hemisphere	3 Mon	Pa	–	–	578 857/1 244 217	8.94/0.04	1
15	M	3	Face	Left	O	11 Mon	Pa	–	–	739 125/887 628	3.66/0.03	1

Abbreviations: CP, complex partial seizure; F, frontal lobe; Fe, female; GL, glaucoma; ID, intellectual disability; LAs, leptomeningeal angiomas; M, male; mon, months; O, occipital lobe; P, parietal lobe; Pa, partial seizure; PWS, port-wine stain; SWS, Sturge–Weber syndrome; T, temporal lobe.
[a]Percent of mutant allele frequency was calculated by mutant allele reads/total reads.

Table 2 Primer sequences for PCR amplification of *GNAQ*

Exon	*Forward (5′–3′)*	*Reverse (5′–3′)*	*Size (bp)*
1	GACACCCCGGTGAATGAG	GGACACGAAAAGGAACAAGC	849
2	AAAAGATGCTGTTGCCATTG	CCAAATATGCCTTTCATTGA	755
3	GATGGGAGAGCTGAATACGC	AGTTTGCAATTTGGGGGAGG	715
4	TTGCCTCTGGGGAGTATGAG	CGATTTTACTCAACCA-CAAGCA	971
5	TACCATTTTGCTTGGCACAG	GACACACCCATCACACAAAC	814
6	TGACAGTGTTCCAGATTCA-CAA	GGAATGCAATGTTTTGTGTCA	650
7	GCCTTGGCTTTCAAGTCATC	GAATTAGCGGGGGAAGAAAA	814

GNAQ (NM_002072.4) gene covering the coding region, intron–exon boundaries, as well as 5′- and 3′-untranslated regions (Table 2). A dual-indexed sequencing library was prepared with the Nextera DNA Sample Preparation Kit (Agilent Technologies) and sequenced on an Illumina MiSeq (Illumina) with 150-bp paired-end reads. Read alignment, sorting and indexing were performed as described above. Somatic single-nucleotide variant calling was performed by MuTect algorithms with the default setting.[8] Variants that passed the MuTect filters were annotated using ANNOVAR software.[9] Novel somatic single-nucleotide variants were selected based on the following four criteria: (1) mutant alleles observed with ≥ 2 reads in the brain and <2 reads in blood leukocytes, (2) variants unregistered in dbSNP 137 except for clinically associated single-nucleotide polymorphisms (flagged),[9] (3) variants unregistered in 6500 ESP, 1000 Genomes databases[10,11] or 575 in-house control exomes and (4) non-synonymous variants.

RESULTS AND DISCUSSION

The recurrent somatic *GNAQ* c.548G>A mutation was identified in 12 of 15 SWS samples (80%) in the present study. The total read depth ranged from 20 284× to 2 674 940× (mean depth, 708 528×). Mutant allele frequencies ranged from 3.66 to 8.94% (mean, 5.59%; Table 1). In the remaining three subjects without c.548G>A (patients 3, 4 and 11; Table 1), we performed *GNAQ* mutation screening. The mean depth of coverage of the coding sequences ranged from 18 080 to 27 967 (average 23 050.6), and 500 or more reads covered 100% of coding sequences. However, no other somatic mutations were found in *GNAQ*.

Heterotrimeric G-proteins are composed of three subunits, α, β and γ, and act as signal transducers when coupled with seven transmembrane receptors in a diverse range of signaling pathways.[12,13] *GNAQ* encodes the q class of G-α subunit that activates phospholipase Cβ, thereby leading to the generation of inositol triphosphate and diacylglycerol.[14,15] Somatic mutations in *GNAQ* were previously reported as oncogenic gain-of-function mutations causing melanocytic neoplasms including melanomas and nevi.[16–18]

Van Raamsdonk *et al.*[17] showed that somatic mutations in the Q209 and R183 residues of GNAQ, especially the Q209L substitution located in the Ras-like domain, were likely to be involved in tumorigenesis through upregulation of the MAP kinase pathway. R183 is located in the GTP-binding pocket of the G-α subunit and has an important role in GTP hydrolysis; however, the potential of the R183 mutant to activate signal transmission was markedly lower than that of the Q209 mutant.[19,20] Recently, Shirley *et al.*[4] identified the somatic *GNAQ* mutation c.548G>A (pR183Q) in 88% of SWS patients (23 of 26) and 92% of patients with non-syndromic port-wine stains (12 of 13). This substitution was suggested to induce moderate activation of the extracellular signal-regulated kinase (ERK) pathway, which may lead to pathologic but not significantly neoplastic growth of capillaries in the skin and brain. In this study, we found the same recurrent somatic c.548G>A (pR183Q) mutation in 80% of patients (12 of 15), which supports the previous findings. However, we could not identify any other causative somatic mutation in *GNAQ*. Therefore it remains unclear whether mutations in other genes can be causative of SWS, although the recurrent somatic *GNAQ* mutation c.548G>A (p.R183Q) appears to be the major determinant in this disorder.

CONFLICT OF INTEREST

The authors declare no conflict of interest.

ACKNOWLEDGEMENTS

We thank the patients for participating in this work. We also thank Nobuko Watanabe for technical assistance. This study was supported by the Ministry of Health, Labour and Welfare of Japan, a Grant-in-Aid for Scientific Research (A), (B) and (C) from the Japan Society for the Promotion of Science, the Takeda Science Foundation, the fund for Creation of Innovation Centers for Advanced Interdisciplinary Research Areas Program in the Project for Developing Innovation Systems, the Strategic Research Program for Brain Sciences and a Grant-in-Aid for Scientific Research on Innovative Areas (Transcription Cycle) from the Ministry of Education, Culture, Sports, Science and Technology of Japan.

1 Sudarsanam, A., Ardern-Holmes, S. L. Sturge-Weber syndrome: from the past to the present. *Eur. J. Paediatr. Neurol.* **18**, 257–266 (2014).
2 Comi, A. M. Update on Sturge-Weber syndrome: diagnosis, treatment, quantitative measures, and controversies. *Lymphat. Res. Biol.* **5**, 257–264 (2007).
3 Huq, A. H., Chugani, D. C., Hukku, B., Serajee, F. J. Evidence of somatic mosaicism in Sturge-Weber syndrome. *Neurology* **59**, 780–782 (2002).
4 Shirley, M. D., Tang, H., Gallione, C. J., Baugher, J. D., Frelin, L. P., Cohen, B. *et al.* Sturge-Weber syndrome and port-wine stains caused by somatic mutation in GNAQ. *New Engl. J. Med.* **368**, 1971–1979 (2013).
5 Li, H., Handsaker, B., Wysoker, A., Fennell, T., Ruan, J., Homer, N. *et al.* The Sequence Alignment/Map format and SAMtools. *Bioinformatics* **25**, 2078–2079 (2009).
6 Robinson, J. T., Thorvaldsdottir, H., Winckler, W., Guttman, M., Lander, E. S., Getz, G. *et al.* Integrative genomics viewer. *Nat. Biotechnol.* **29**, 24–26 (2011).
7 Thorvaldsdottir, H., Robinson, J. T., Mesirov, J. P. Integrative Genomics Viewer (IGV): high-performance genomics data visualization and exploration. *Brief Bioinform.* **14**, 178–192 (2013).
8 Cibulskis, K., Lawrence, M. S., Carter, S. L., Sivachenko, A., Jaffe, D., Sougnez, C. *et al.* Sensitive detection of somatic point mutations in impure and heterogeneous cancer samples. *Nat. Biotechnol.* **31**, 213–219 (2013).
9 Wang, K., Li, M., Hakonarson, H. ANNOVAR: functional annotation of genetic variants from high-throughput sequencing data. *Nucleic Acids Res.* **38**, e164 (2010).
10 Genomes Project C., Abecasis, G. R., Altshuler, D., Auton, A., Brooks, L. D., Durbin, R. M. *et al.* A map of human genome variation from population-scale sequencing. *Nature* **467**, 1061–1073 (2010).
11 Genomes Project C., Abecasis, G. R., Auton, A., Brooks, L. D., DePristo, M. A., Durbin, R. M. *et al.* An integrated map of genetic variation from 1,092 human genomes. *Nature* **491**, 56–65 (2012).
12 Neves, S. R., Ram, P. T., Iyengar, R. G protein pathways. *Science* **296**, 1636–1639 (2002).
13 McCudden, C. R., Hains, M. D., Kimple, R. J., Siderovski, D. P., Willard, F. S. G-protein signaling: back to the future. *Cell Mol. Life Sci.* **62**, 551–577 (2005).
14 Dong, Q., Shenker, A., Way, J., Haddad, B. R., Lin, K., Hughes, M. R. *et al.* Molecular cloning of human G alpha q cDNA and chromosomal localization of the G alpha q gene (GNAQ) and a processed pseudogene. *Genomics* **30**, 470–475 (1995).
15 Mizuno, N., Itoh, H. Functions and regulatory mechanisms of Gq-signaling pathways. *Neurosignals* **17**, 42–54 (2009).
16 Van Raamsdonk, C. D., Bezrookove, V., Green, G., Bauer, J., Gaugler, L., O'Brien, J. M. *et al.* Frequent somatic mutations of GNAQ in uveal melanoma and blue naevi. *Nature* **457**, 599–602 (2009).
17 Van Raamsdonk, C. D., Griewank, K. G., Crosby, M. B., Garrido, M. C., Vemula, S., Wiesner, T. *et al.* Mutations in GNA11 in uveal melanoma. *New Engl. J. Med.* **363**, 2191–2199 (2010).
18 Wu, D., Katz, A., Lee, C. H., Simon, M. I. Activation of phospholipase C by alpha 1-adrenergic receptors is mediated by the alpha subunits of Gq family. *J. Biol. Chem.* **267**, 25798–25802 (1992).
19 Orth, J. H., Preuss, I., Fester, I., Schlosser, A., Wilson, B. A., Aktories, K. Pasteurella multocida toxin activation of heterotrimeric G proteins by deamidation. *Proc. Natl Acad. Sci. USA* **106**, 7179–7184 (2009).
20 O'Hayre, M., Vazquez-Prado, J., Kufareva, I., Stawiski, E. W., Handel, T. M., Seshagiri, S. *et al.* The emerging mutational landscape of G proteins and G-protein-coupled receptors in cancer. *Nat. Rev. Cancer* **13**, 412–424 (2013).

Neurogenetics (2014) 15:193–200
DOI 10.1007/s10048-014-0408-y

ORIGINAL ARTICLE

Novel compound heterozygous *PIGT* mutations caused multiple congenital anomalies-hypotonia-seizures syndrome 3

Mitsuko Nakashima · Hirofumi Kashii · Yoshiko Murakami · Mitsuhiro Kato · Yoshinori Tsurusaki · Noriko Miyake · Masaya Kubota · Taroh Kinoshita · Hirotomo Saitsu · Naomichi Matsumoto

Received: 21 February 2014 / Accepted: 25 May 2014 / Published online: 8 June 2014

Abstract Recessive mutations in genes of the glycosylphosphatidylinositol (GPI)-anchor synthesis pathway have been demonstrated as causative of GPI deficiency disorders associated with intellectual disability, seizures, and diverse congenital anomalies. We performed whole exome sequencing in a patient with progressive encephalopathies and multiple dysmorphism with hypophosphatasia and identified novel compound heterozygous mutations, c.250G>T (p. Glu84*) and c.1342C>T (p. Arg488Trp), in *PIGT* encoding a subunit of the GPI transamidase complex. The surface expression of GPI-anchored proteins (GPI-APs) on patient granulocytes was lower than that of healthy controls. Transfection of the Arg488Trp mutant *PIGT* construct, but not the Glu84* mutant, into PIGT-deficient cells partially restored the expression of GPI-APs DAF and CD59. These results indicate that *PIGT* mutations caused neurological impairment and multiple congenital anomalies in this patient.

M. Nakashima · Y. Tsurusaki · N. Miyake · H. Saitsu · N. Matsumoto (✉)
Department of Human Genetics, Yokohama City University Graduate School of Medicine, 3-9 Fukuura, Kanazawa-ku, Yokohama 236-0004, Japan
e-mail: naomat@yokohama-cu.ac.jp

H. Kashii · M. Kubota
Division of Neurology, National Center for Child Health and Development, Tokyo, Japan

Y. Murakami · T. Kinoshita
Research Institute for Microbial Diseases and World Premier International Immunology Frontier Research Center, Osaka University, Osaka, Japan

M. Kato
Department of Pediatrics, Yamagata University Faculty of Medicine, Yamagata, Japan

Keywords Whole exome sequencing · *PIGT* · Compound heterozygous mutations · Glycosylphosphatidylinositol-anchored protein · Multiple congenital anomalies-hypotonia-seizures syndrome 3 · Hypophosphatasia

Introduction

Glycosylphosphatidylinositol (GPI) acts as the anchor of various eukaryotic proteins expressed on the plasma membrane. GPI synthesis and GPI-anchored protein (GPI-AP) modification are mediated by at least 27 genes in the endoplasmic reticulum (ER) and Golgi apparatus [1]. Recent studies have indicated that inherited loss-of-function mutations in these genes lead to GPI deficiencies associated with neurological impairments including seizures, intellectual disability, and multiple congenital anomalies [2–9]. In addition, somatic mutations in PIGA cause paroxysmal nocturnal haemoglobinuria, a haematopoietic disease, which is also caused by somatic mutation of PIGT in combination with the germ line mutation of one allele [10, 11].

PIGT is one of the subunits of the GPI transamidase complex, and catalyzes the attachment of GPI anchors to proteins in the ER [1]. Kvarnung et al. [12] previously reported a homozygous *PIGT* mutation in patients from a consanguineous Turkish family with multiple congenital anomalies-hypotonia-seizures syndrome-3 (MCAHS3 [MIM 615398]). In the present study, we describe the use of whole exome sequencing to identify novel compound heterozygous *PIGT* mutations in a Japanese patient with seizures, intellectual disability and multiple congenital anomalies. Functional analysis indicated that these mutations are causative of GPI deficiency.

Patient and methods

Patient

The female proband was born at full term without asphyxia as the first child of healthy unrelated parents (Fig. 1a). Polyhydramnios was recognized during pregnancy. She showed poor sucking and post-feed stridor soon after birth. At 4 months of age, she showed tonic seizures with apnea and myoclonic seizures, both of which repeatedly turned to convulsive status. Her electroencephalogram (EEG) demonstrated high-amplitude slow wave as a background activity, but no epileptic discharges were observed. She also showed a poor response, muscle hypotonia, unstable head control, a cardiac murmur caused by patent ductus arteriosus, and left hydronephroureter with ureteral stenosis. Her seizures were refractory to multiple antiepileptic drugs such as carbamazepine, clobazam, and an intravenous injection of pyridoxal phosphate while the frequency of her seizures decreased with the combination of valproic acid, zonisamide, and phenytoin to some extent. Phenobarbital could not be used in infancy because of drug eruption. After 1 year of age, she was frequently admitted to hospital because of convulsive status epilepticus induced by fever, or recurrent episodes of respiratory infections, bronchial asthma, or gastroenteritis. Her sleep cycle was disorganized. Brain magnetic resonance imaging at 3 years of age demonstrated progressive atrophy of the cerebral hemisphere, cerebellum, and brainstem (Fig. 1c). EEG at 3 years showed borderline findings consisting of a predominance of fast wave activity with no spindle formation interrupted by slow wave burst. She recurrently suffered bone fractures without obvious event. Systemic bone X-ray at 12 years of age showed neurogenic arthrogryposis and osteoporosis. At 12 years of age, she was bedridden and was only able to roll over. She showed profound intellectual disability and had no meaningful words. Her epileptic seizures disappeared after 10 years of age, but epileptic discharges comprised of spike-and-slow wave complex at bilateral frontal area with low-amplitude irregular background activity were seen on EEG.

G-banded chromosomal analysis revealed a normal karyotype (46,XX). Metabolic screenings including amino acids, lactic acid, pyruvic acid, organic acids, lactic acid, and lysosomal enzymes were unremarkable. The biochemical analysis of blood repeatedly showed low levels of serum alkaline phosphatase from birth (186 U/l at birth and 326 U/l at 7 years of age [normal range, 450–1250 U/l]). Both concentrations of serum and urine calcium were normal (serum calcium, 9.6 mg/dl; U-calcium/U-creatinine ratio, 0.23 at 7 years of age).

DNA preparation

Peripheral blood samples were obtained from the patient and her parents after parents signed informed consent. DNA was extracted using QuickGene-610 L (Fujifilm, Tokyo, Japan) according to the manufacturer's instructions. The study was approved by the ethics committee of the Yokohama City University.

Whole exome sequencing

Patient DNA was captured with the SureSelect Human All Exon V5 Kit (Agilent Technologies, Santa Clara, CA, USA) and sequenced on an Illumina Hiseq2000 (Illumina, San Diego, CA, USA) with 101-bp paired-end reads. Image analysis and base calling were performed by sequence control software real-time analysis and CASAVA software v1.8 (Illumina). Reads were mapped to the human reference genome sequence (UCSC hg19, NCBI build 37) and aligned using Novoalign (Novocraft Technologies, Jaya, Malaysia). PCR duplicate reads were excluded using Picard (http://picard.sourceforge.net/) for further analysis. Single-nucleotide variants (SNVs) and small indels were identified using the Genome Analysis Toolkit UnifiedGenotyper [13] and filtered according to the Broad Institute's best-practice guidelines (version 3). Variants that passed the filters were annotated using ANNOVAR[14]. The damaging prediction was performed by Polyphen-2 [15] and MutationTaster software [16].

Sanger sequencing

PIGT exon 2 and exon 10 sequences were PCR amplified from the patient and her parents using the following primers: *PIGT* ex2F 5′-GGGAGGAACTTGTCATCACC-3′ and ex2R 5′-CAGTGGCAGGATGACAACAC-3′, *PIGT* ex10F 5′-AGAGATGTGGGTGACCTTGC-3′ and ex10R 5′-CTGAGGACAGATGGGCTACA-3′, respectively. Amplified PCR products were sequenced on an ABI 3500xl or 3130xl Genetic Analyzer (Applied Biosystems, Foster City, CA, USA).

Flow cytometry

Peripheral blood samples were collected from the patient and normal control individuals. Granulocyte surface expression of total GPI-APs was quantified by staining with Alexa 488-conjugated inactivated aerolysin (FLAER; Protox Biotech, Victoria, Canada). Expression of CD16, CD24, and alkaline phosphatase (ALP) was examined using appropriate primary antibodies (3G8, ML5, and B4-78, respectively; BD Biosciences, Franklin Lakes, NJ, USA), followed by a PE-conjugated anti-mouse IgG secondary antibody (BD Biosciences). Cells were analyzed by BD FACSCanto II (BD Biosciences).

Human *PIGT* cDNA (NM_015937.5) with FLAG at the C terminus was subcloned into the pME (driven by a strong SRα promoter) or pTA (driven by a weak promoter

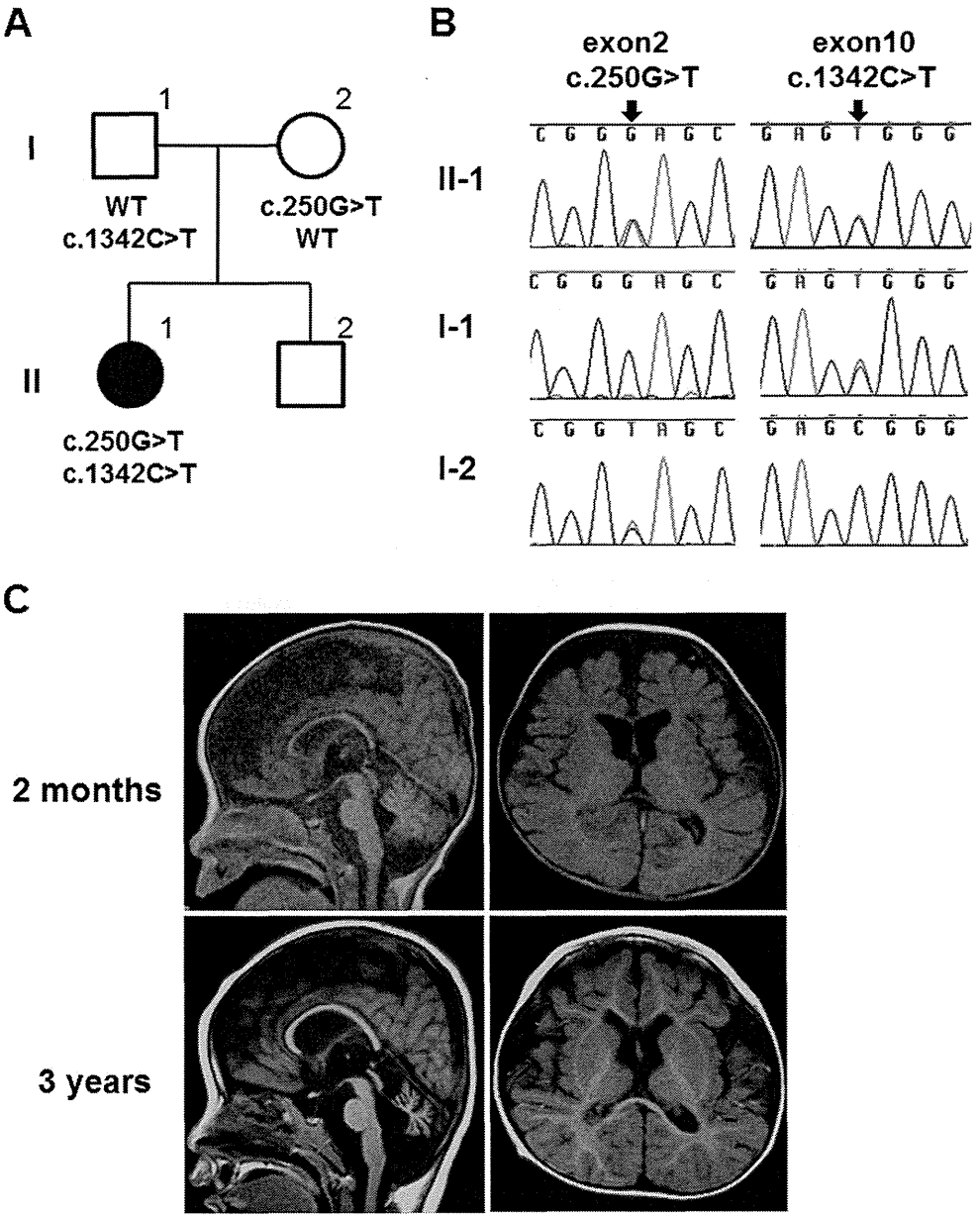

Fig. 1 **a** Familial pedigree. **b** Sanger sequencing results. Compound heterozygous mutations, c.250G>T and c.1342C>T, in *PIGT* were observed in the affected individual. c.250G>T (*left*) and c.1342C>T (*right*) were inherited from the mother and the father, respectively. **c** Magnetic resonance imaging of the patient's brain. Axial and sagittal T1-weighted images at 3 years of age show atrophic changes of the cerebral hemisphere, brainstem, and cerebellum

containing only TATA-box) vector [17]. Two *PIGT* mutants, Glu84* and Arg488Trp, were generated by site-directed mutagenesis. Mutant and wild-type *PIGT* plasmids were transfected by electroporation into CHO H4, *PIGT*-deficient Chinese hamster ovary (CHO) cells expressing human DAF (also called CD55) and CD59 as previously described [18]. Two days later, lysates were run on SDS-PAGE, and Western blotting was performed using an anti-FLAG antibody (M2; Sigma-Aldrich, St. Louis, MO, USA) to detect FLAG-tagged PIGT (PIGT-F). The protein levels were normalized to the loading control, and luciferase activities were used to evaluate transfection efficiencies. Cells were stained with anti-hCD59 (5H8), anti-hDAF (IA10), and anti-Hamster uPAR (5D6) antibodies and restoration of the surface expression of GPI-APs was assessed by flow cytometry.

Results

Mutation screening

We performed mutation screening for previously reported genes involved in the GPI-anchor–synthesis pathway, and identified the compound heterozygous mutations c.250G>T (p. Glu84*) and c.1342C>T (p. Arg488Trp) in *PIGT* (NM_015937.5). Both mutations were not found in 6500

ESP (Exome Sequencing Project) or 1000 genomes [19, 20], but c.1342C>T is present in one of 408 in-house control exomes. Both mutations were predicted to be probably disease-causing by Polyphen-2 and MutationTaster. Sanger sequencing confirmed that c.250G>T and c.1342C>T were inherited from the mother and father, respectively (Fig. 1b).

Functional effect of the mutations on GPI synthesis

PIGT is a component of GPI transamidase that mediates the post-translational attachment of GPI anchors to the C-terminal of the precursor protein. Therefore, the mutant GPI transamidase is likely to impair the surface expression of GPI-APs. To investigate the influence of *PIGT* mutations on GPI-APs synthesis, we first examined the granulocyte surface expression of GPI-APs from the patient and a healthy control. Expression of total GPI-APs (FLAER staining) and GPI-APs CD16 and ALP on granulocytes was reduced in the patient compared to the normal control (Fig. 2a). However, similar expression levels of another GPI-AP CD24 were seen in the patient and control (Fig. 2a).

We then transiently transfected wild-type or mutant (Glu84* or Arg488Trp) *PIGT* cDNA constructs into *PIGT*-deficient CHO cells to evaluate the functional effect of each mutation on GPI-AP expression. Western blotting revealed that the expression level of Arg488Trp mutant protein was similar to that of wild-type protein, whereas the Glu84* mutant expressed a small amount of full-length protein (probably read-though) (Fig. 2c). Wild-type *PIGT* transfection successfully restored the expression of GPI-APs CD59, DAF (CD55), and uPAR in both cases using vectors with a strong (pME) and weak (pTA) promoter (Fig. 2b). The Arg488Trp mutant *PIGT* cloned in pME restored the expression of GPI-APs close to that of wild-type, whereas the same mutant in the pTA vector only partially restored expression. The Glu84* mutant *PIGT* in the pME vector insufficiently restored the expression of GPI-APs, while this mutant in the pTA vector could not restore expression (Fig. 2b). These results demonstrate that both mutants, especially the Glu84* alteration, reduce the activity of PIGT function.

Fig. 2 **a** Surface expression of GPI-APs on granulocytes. Granulocytes from the patient and healthy control were stained with FLAER or antibodies against CD24, CD16, and ALP. The expression of total GPI, CD16, and ALP in the patient (*solid line*) was lower than in the normal control (*dark shaded area*). CD24 expression did not differ between the patient and control. The *light shaded areas* represent the isotype control. *X* axes show fluorescent intensities, which indicate expression levels of each GPI-AP on the cell surface. *Y* axes show the relative cell numbers. The value of mean fluorescent intensities of each sample is shown in each panel. **b** PIGT-deficient CHO cells were transiently transfected with wild-type (*dashed line*), Glu84* mutant (*fine solid line*), or Arg488Trp mutant (*bold solid line*) *PIGT* cDNA expression constructs in vectors with either a strong promoter (pME; *upper panels*) or weak promoter (pTA; *lower panels*). PIGT-F protein levels and restoration of the surface expression of CD59, DAF, and uPAR were assessed 2 days later. The *dark* and *light shadows* represent empty-vector transfectants and isotype controls, respectively. **c** Western blotting showed that the Arg488Trp mutant protein was expressed at similar levels to the wild-type protein, whereas the Glu84* mutant full-length protein, representing the read-through product, was expressed at lower levels. Quantity numbers at the bottom of the gel indicate the relative intensity of PIGT-F protein levels normalized to the loading control, and luciferase activities used for evaluating transfection efficiencies. *Arrowhead* indicates a non-specific product

Discussion

GPI deficiency syndromes are recessive disorders caused by mutations in genes involved in the GPI-anchor biosynthesis pathway. Here, we describe novel compound heterozygous *PIGT* mutations in a nonconsanguineous patient presenting with seizures and intellectual disability.

The first reported *PIGT* mutation (c.547A>C, p.Thr183Pro) was identified in a consanguineous Turkish family who showed seizures, intellectual disability, and multiple congenital anomalies [12]. A decreased expression of GPI-APs was documented on patient granulocytes. They confirmed that the homozygous c.547A>C mutation impaired the function of PIGT by the functional study using *pigt* knockdown zebrafish embryos which showed gastrulation defects phenotype. In the present study, we also demonstrated that both *PIGT* mutations, c.250G>T (p. Glu84*) and c.1342C>T (p. Arg488Trp), impaired the function of PIGT which was confirmed by the functional study using the PIGT deficient CHO cells.

Mammalian GPI transamidase consists of at least five subunits, PIGK, GPAA1, PIGS, PIGT, and PIGU [1]. Of these, PIGT plays a critical role in stabilizing the complex formation of GPI transamidase [17], which mediates cleavage of the GPI attachment signal peptide at the C-terminal of the precursor protein and transfers GPI anchors to the C-terminal of cleaved proteins [1]. Consequently, PIGT mutants may not be able to correctly form the GPI transamidase complex, leading to a loss of GPI transamidase activity and reduction in the cellular surface expression of GPI-APs.

Our patient and four patients described by Kvarnung et al. [12] showed broad clinical spectrum and shared several common features (Table 1). The neurological findings including intractable seizures, hypotonia and severe intellectual disability were observed in all patients. Ophthalmologic features including strabismus, nystagmus, and cerebral visual impairment were also observed in all. Cerebral and cerebellar atrophy was observed in our patient and two of four seen by Kvarnung et al. The EEG findings in our patient were also exacerbated as she grew, suggesting progressive encephalopathy. Our patient and three of four patients by Kvarnung et al. had some cardiologic disorders. All patients had some

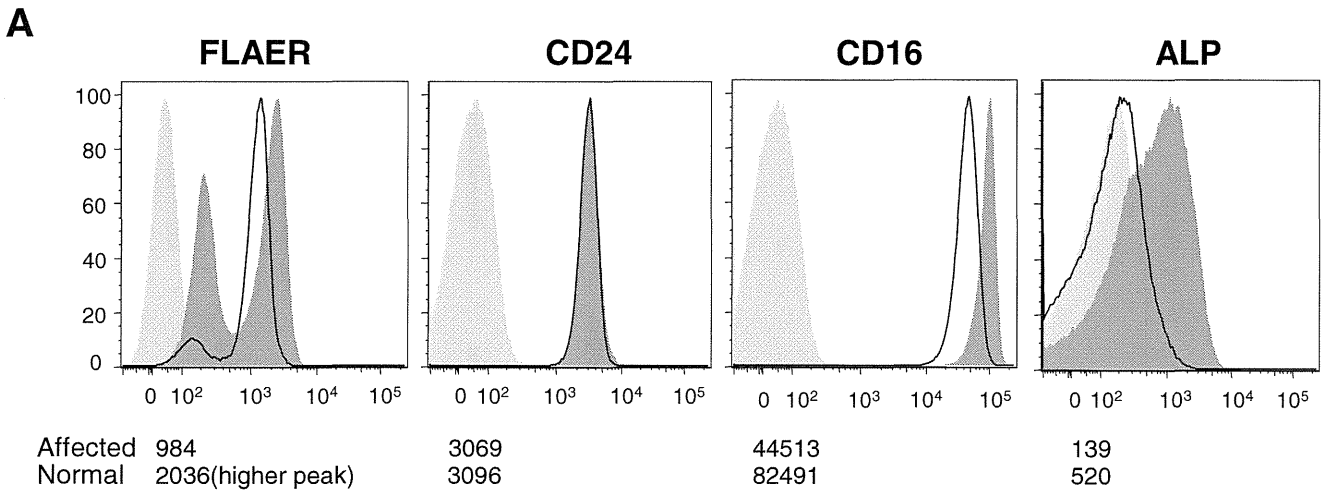
A
FLAER
CD24
CD16
ALP
100
80
60
40
20
0
0 10² 10³ 10⁴ 10⁵
Affected 984 3069 44513 139
Normal 2036(higher peak) 3096 82491 520

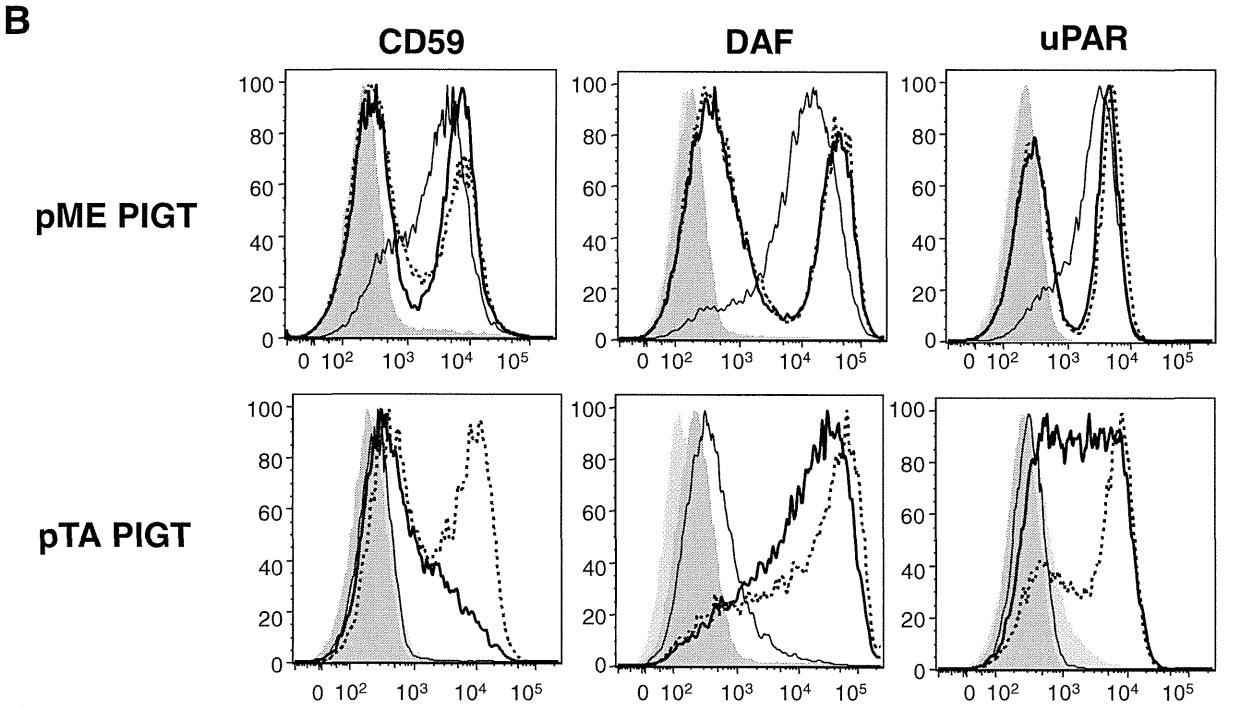
B
CD59
DAF
uPAR
pME PIGT
pTA PIGT
100
80
60
40
20
0
0 10² 10³ 10⁴ 10⁵

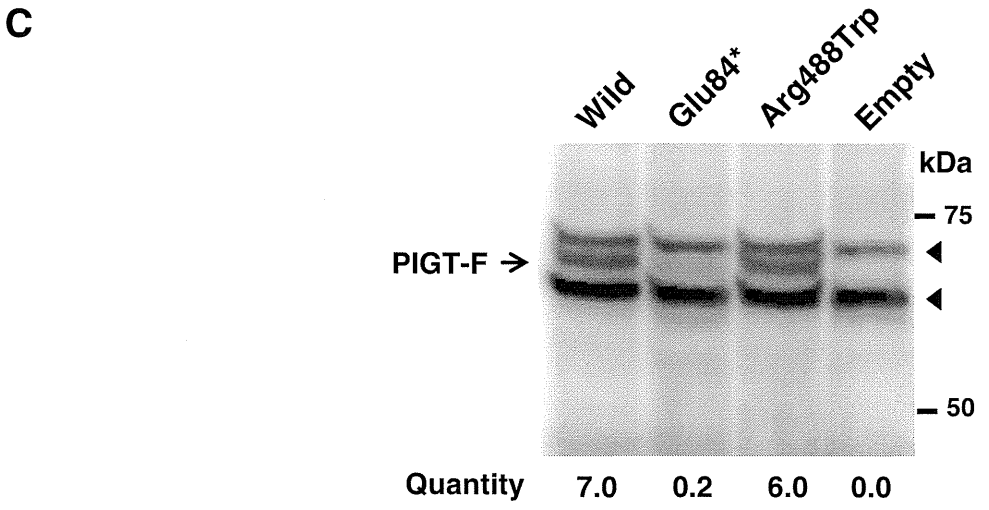
C
Wild
Glu84*
Arg488Trp
Empty
kDa
75
50
PIGT-F
Quantity 7.0 0.2 6.0 0.0

Table 1 Clinical features of patients with PIGT mutations

Patients	This Patient	Kvarnung et al. Patient 1	Kvarnung et al. Patient 2	Kvarnung et al. Patient 3	Kvarnung et al. Patient 4
consanguinity	–	+	+	+	+
Sex	Female	Female	Female	Female	Female
Gestation	40 weeks	40 weeks	39 weeks	37 weeks	37 weeks
Birth weight	3,816 g	4,735 g	4,500 g	3,460 g	3,240 g
Birth length	51 cm	53 cm	54 cm	53 cm	53 cm
BHC	35.5 cm +1.8 SD	38 cm +2 SD	39 cm +3 SD	35 cm +1 SD	36 cm +1.5 SD
HPP	+	+	+	+	+
ID	+	+	+	+	+
Hypotonia	+	+	+	+	+
Seizure	+	+	+	+	+
Strabismus	+	+	+	+	+
Nystagmus	+	+	+	+	+
CVI	+	+	+	+	+
Brain images	CT: dilated ventricle, frontal atrophy, cerebellar and brainstem atrophy	CT: primitive Sylvian fissures	CT: Normal findings	MRI: global atrophy with predominate vermis and cerebellar atrophy, atrophy of basal ganglia	MRI: global atrophy with predominat vermis and cerebellar atrophy, hypomyelination
Tooth abnormalities	–	+	+	+	+
Skeletal features	Scoliosis, osteoporosis	Craniosynostosis, Pectus excavatum, Short arm, Scoliosis, Delayed bone age, Reduced mineralisation	Craniosynostosis, short arm, Scoliosis, Delayed bone age, Reduced mineralisation	Short arm, Delayed bone age, Reduced mineralisation	Short arm, Delayed bone age, Reduced mineralisation
Urologic features	Urolithiasis, Ureteral dilation	Nephrocalcinosis	Nephrocalcinosis, Ureteral dilation, Cysts and dysplasia	Nephrocalcinosis, Ureteral dilation	Nephrocalcinosis, Ureteral dilation
Cardiologic features	PDA	Minor PDA	–	Mild restrictive CMP	Increased atrial load on ECG
Facial features	Low set ears, micrognathia, malar flattening, upslanting palpebral fissures, depressed nasal bridge, short anteverted nose, downturned corners of the mouth, tented lip, high arched palate	High forehead with bitemporal narrowing, broad nasal root, anteverted nose, long philtrum with a deep groove, distinct cupid bow	High forehead with bitemporal narrowing, broad nasal root, anteverted nose, long philtrum with a deep groove, distinct cupid bow	High forehead with bitemporal narrowing, broad nasal root, anteverted nose, long philtrum with a deep groove, distinct cupid bow	High forehead with bitemporal narrowing, broad nasal root, anteverted nose, long philtrum with a deep groove, distinct cupid bow

BHC birth head circumference, *HPP* hypophosphatasia, *ID* intellectual disability, *CVI* cerebral visual impairment, *ECG* electrocardiogram, *CMP* cardiomyopathy, *PDA* patent ductus arteriosus

urologic features, but not nephrocalcinosis in our patient. Our case shared similar facial features with previous patients including a depressed nasal bridge, short anteverted nose, tented lip, and downturned corners of the mouth. Low set ears, micrognathia, malar flattening, and upslanting palpebral fissures were unique to our patient.

Hyperphosphatasia is a characteristic symptom of some GPI deficiencies, such as PIGV, PIGW, PIGO, PGAP2 and PGAP3 deficiencies [2–6]. In contrast, hypophosphatasia is a particularly distinctive feature in the loss of GPI transamidase function. Murakami at al. suggested that GPI transamidase abnormalities lead to an inability to hydrolyze the precursor protein of alkaline phosphatase, resulting in the degradation of most precursor proteins within the cell and a decrease of serum alkaline phosphatase levels (hypophosphatasia) [21]. This is supported in our case by the hypophosphatasia. The patients described by Kvarnung et al. showed hypercalcemia and hypercalciuria following tooth abnormality, craniosynostosis, a delayed bone age, and reduced mineralization, which is the common features with infantile hypophosphatasia caused by the mutations in *ALPL*, the gene encoding tissue non-specific alkaline phosphatase (TNAP) [22]. As TNAP is a GPI-AP, the PIGT deficiency causes decreased surface expression of TNAP, which would lead to bone abnormalities. Regardless of hypophosphatasia, our case showed only mild scoliosis and osteoporosis, but no tooth abnormality nor craniosynostosis. Different mutational effects on the enzyme activity may account for such different phenotypes. In this study, mutant PIGT construct harboring Arg488Trp or Glu84* in strong promoter (pME) vector restored GPI-Aps expression. In contrast, Kvarnung et al. showed that abnormal phenotype of pigt knockdown zebrafish was never restored by the homozygous mutant (Thr183Pro) PIGT cDNA. Therefore, it is possible to estimate that the Thr183Pro mutation may affect the GPI transamidase complex activity more severely than the Arg488Trp and Glu84* mutations, leading to less severe phenotypes. However, further functional analysis and cases with *PIGT* mutations are needed to elucidate the relevance of these mutations in PIGT function and full clinical spectrum of GPI deficiency syndromes.

Acknowledgments We thank the patient's family for participating in this work. We also thank Nobuko Watanabe for her technical assistance. This study was supported by the Ministry of Health, Labour and Welfare of Japan, a Grant-in-Aid for Scientific Research (A), (B), and (C) from the Japan Society for the Promotion of Science, the Takeda Science Foundation, the fund for Creation of Innovation Centers for Advanced Interdisciplinary Research Areas Program in the Project for Developing Innovation Systems, the Strategic Research Program for Brain Sciences, and a Grant-in-Aid for Scientific Research on Innovative Areas (Transcription Cycle) from the Ministry of Education, Culture, Sports, Science and Technology of Japan.

Conflict of interest The authors declare that they have no conflict of interest.

References

1. Kinoshita T, Fujita M, Maeda Y (2008) Biosynthesis, remodelling and functions of mammalian GPI-anchored proteins: recent progress. J Biochem 144(3):287–294. doi:10.1093/jb/mvn090
2. Krawitz PM, Schweiger MR, Rodelsperger C, Marcelis C, Kolsch U, Meisel C, Stephani F, Kinoshita T, Murakami Y, Bauer S, Isau M, Fischer A, Dahl A, Kerick M, Hecht J, Kohler S, Jager M, Grunhagen J, de Condor BJ, Doelken S, Brunner HG, Meinecke P, Passarge E, Thompson MD, Cole DE, Horn D, Roscioli T, Mundlos S, Robinson PN (2010) Identity-by-descent filtering of exome sequence data identifies PIGV mutations in hyperphosphatasia mental retardation syndrome. Nat Genet 42(10):827–829. doi:10.1038/ng.653
3. Krawitz PM, Murakami Y, Hecht J, Kruger U, Holder SE, Mortier GR, Delle Chiaie B, De Baere E, Thompson MD, Roscioli T, Kielbasa S, Kinoshita T, Mundlos S, Robinson PN, Horn D (2012) Mutations in PIGO, a member of the GPI-anchor-synthesis pathway, cause hyperphosphatasia with mental retardation. Am J Hum Genet 91(1):146–151. doi:10.1016/j.ajhg.2012.05.004
4. Hansen L, Tawamie H, Murakami Y, Mang Y, ur Rehman S, Buchert R, Schaffer S, Muhammad S, Bak M, Nothen MM, Bennett EP, Maeda Y, Aigner M, Reis A, Kinoshita T, Tommerup N, Baig SM, Abou Jamra R (2013) Hypomorphic mutations in PGAP2, encoding a GPI-anchor-remodeling protein, cause autosomal-recessive intellectual disability. Am J Hum Genet 92(4):575–583. doi:10.1016/j.ajhg.2013.03.008
5. Howard MF, Murakami Y, Pagnamenta AT, Daumer-Haas C, Fischer B, Hecht J, Keays DA, Knight SJ, Kolsch U, Kruger U, Leiz S, Maeda Y, Mitchell D, Mundlos S, Phillips JA 3rd, Robinson PN, Kini U, Taylor JC, Horn D, Kinoshita T, Krawitz PM (2014) Mutations in PGAP3 impair GPI-anchor maturation, causing a subtype of hyperphosphatasia with mental retardation. Am J Hum Genet 94(2):278–287. doi:10.1016/j.ajhg.2013.12.012
6. Chiyonobu T, Inoue N, Morimoto M, Kinoshita T, Murakami Y (2013) Glycosylphosphatidylinositol (GPI) anchor deficiency caused by mutations in PIGW is associated with West syndrome and hyperphosphatasia with mental retardation syndrome. J Med Genet. doi:10.1136/jmedgenet-2013-102156
7. Krawitz PM, Murakami Y, Riess A, Hietala M, Kruger U, Zhu N, Kinoshita T, Mundlos S, Hecht J, Robinson PN, Horn D (2013) PGAP2 mutations, affecting the GPI-anchor-synthesis pathway, cause hyperphosphatasia with mental retardation syndrome. Am J Hum Genet 92(4):584–589. doi:10.1016/j.ajhg.2013.03.011
8. Almeida AM, Murakami Y, Layton DM, Hillmen P, Sellick GS, Maeda Y, Richards S, Patterson S, Kotsianidis I, Mollica L, Crawford DH, Baker A, Ferguson M, Roberts I, Houlston R, Kinoshita T, Karadimitris A (2006) Hypomorphic promoter mutation in PIGM causes inherited glycosylphosphatidylinositol deficiency. Nat Med 12(7):846–851. doi:10.1038/nm1410
9. Ng BG, Hackmann K, Jones MA, Eroshkin AM, He P, Wiliams R, Bhide S, Cantagrel V, Gleeson JG, Paller AS, Schnur RE, Tinschert S, Zunich J, Hegde MR, Freeze HH (2012) Mutations in the glycosylphosphatidylinositol gene PIGL cause CHIME syndrome. Am J Hum Genet 90(4):685–688. doi:10.1016/j.ajhg.2012.02.010
10. Johnston JJ, Gropman AL, Sapp JC, Teer JK, Martin JM, Liu CF, Yuan X, Ye Z, Cheng L, Brodsky RA, Biesecker LG (2012) The phenotype of a germline mutation in PIGA: the gene somatically mutated in paroxysmal nocturnal hemoglobinuria. Am J Hum Genet 90(2):295–300. doi:10.1016/j.ajhg.2011.11.031
11. Krawitz PM, Hochsmann B, Murakami Y, Teubner B, Kruger U, Klopocki E, Neitzel H, Hoellein A, Schneider C, Parkhomchuk D, Hecht J, Robinson PN, Mundlos S, Kinoshita T, Schrezenmeier H (2013) A case of paroxysmal nocturnal hemoglobinuria caused by a

germline mutation and a somatic mutation in PIGT. Blood 122(7): 1312–1315. doi:10.1182/blood-2013-01-481499
12. Kvarnung M, Nilsson D, Lindstrand A, Korenke GC, Chiang SC, Blennow E, Bergmann M, Stodberg T, Makitie O, Anderlid BM, Bryceson YT, Nordenskjold M, Nordgren A (2013) A novel intellectual disability syndrome caused by GPI anchor deficiency due to homozygous mutations in PIGT. J Med Genet 50(8):521–528. doi: 10.1136/jmedgenet-2013-101654
13. DePristo MA, Banks E, Poplin R, Garimella KV, Maguire JR, Hartl C, Philippakis AA, del Angel G, Rivas MA, Hanna M, McKenna A, Fennell TJ, Kernytsky AM, Sivachenko AY, Cibulskis K, Gabriel SB, Altshuler D, Daly MJ (2011) A framework for variation discovery and genotyping using next-generation DNA sequencing data. Nat Genet 43(5):491–498. doi:10.1038/ng.806
14. Wang K, Li M, Hakonarson H (2010) ANNOVAR: functional annotation of genetic variants from high-throughput sequencing data. Nucleic Acids Res 38(16):e164. doi:10.1093/nar/gkq603
15. Adzhubei IA, Schmidt S, Peshkin L, Ramensky VE, Gerasimova A, Bork P, Kondrashov AS, Sunyaev SR (2010) A method and server for predicting damaging missense mutations. Nat Methods 7(4):248–249. doi:10.1038/nmeth0410-248
16. Schwarz JM, Rodelsperger C, Schuelke M, Seelow D (2010) MutationTaster evaluates disease-causing potential of sequence alterations. Nat Methods 7(8):575–576. doi:10.1038/nmeth0810-575
17. Ohishi K, Inoue N, Kinoshita T (2001) PIG-S and PIG-T, essential for GPI anchor attachment to proteins, form a complex with GAA1 and GPI8. EMBO J 20(15):4088–4098. doi:10.1093/emboj/20.15.4088
18. Ashida H, Hong Y, Murakami Y, Shishioh N, Sugimoto N, Kim YU, Maeda Y, Kinoshita T (2005) Mammalian PIG-X and yeast Pbn1p are the essential components of glycosylphosphatidylinositol-mannosyltransferase I. Mol Biol Cell 16(3):1439–1448. doi:10.1091/mbc.E04-09-0802
19. Genomes Project C, Abecasis GR, Altshuler D, Auton A, Brooks LD, Durbin RM, Gibbs RA, Hurles ME, McVean GA (2010) A map of human genome variation from population-scale sequencing. Nature 467(7319):1061–1073. doi:10.1038/nature09534
20. Genomes Project C, Abecasis GR, Auton A, Brooks LD, DePristo MA, Durbin RM, Handsaker RE, Kang HM, Marth GT, McVean GA (2012) An integrated map of genetic variation from 1,092 human genomes. Nature 491(7422):56–65. doi:10.1038/nature11632
21. Murakami Y, Kanzawa N, Saito K, Krawitz PM, Mundlos S, Robinson PN, Karadimitris A, Maeda Y, Kinoshita T (2012) Mechanism for release of alkaline phosphatase caused by glycosylphosphatidylinositol deficiency in patients with hyperphosphatasia mental retardation syndrome. J Biol Chem 287(9):6318–6325. doi:10.1074/jbc.M111.331090
22. Mornet E (2007) Hypophosphatasia. Orphanet J Rare Dis 2:40. doi: 10.1186/1750-1172-2-40

CLINICAL GENETICS An International Journal of Genetics, Molecular and Personalized Medicine

Clin Genet 2013
Printed in Singapore. All rights reserved

CLINICAL GENETICS
doi: 10.1111/cge.12188

Letter to the Editor

AKT3 and *PIK3R2* mutations in two patients with megalencephaly-related syndromes: MCAP and MPPH

To the Editor:

Megalencephaly-capillary malformation syndrome (MCAP) and megalencephaly-polymicrogyria-polyd actyly-hydrocephalus syndrome (MPPH) belong to a spectrum of megalencephaly-related syndromes. The diagnostic criteria for MCAP include megalencephaly plus capillary malformations or syndactyly, and those for MPPH include megalencephaly and polymicrogyria, an absence of vascular anomalies, syndactyly, and brain heterotopia (1). Recently, *AKT3*, *PIK3R2*, and *PIK3CA* mutations have been identified in MCAP and MPPH (2). The proteins encoded by these genes are core components of the phosphatidylinositol 3-kinase (PI3K)-AKT pathway (3). Here, we report two patients with an *AKT3* and *PIK3R2* mutation. The study protocol was approved by the Institutional Review Boards for Ethical Issues at Yokohama City University and Yamagata University.

Patient 1 is an 8-year-old girl who has been previously reported as having MPPH (4). Brain magnetic resonance imaging (MRI) at 6 years showed asymmetry of the gyral pattern, dilated lateral ventricles, polymicrogyria, and abnormal signals in the occipital lobes, suggesting dysmyelination (Fig. 1a–c). Patient 2 is a 2-month-old boy who showed macrocephaly, cutis marmorata of the distal extremities, and hyperextensibility

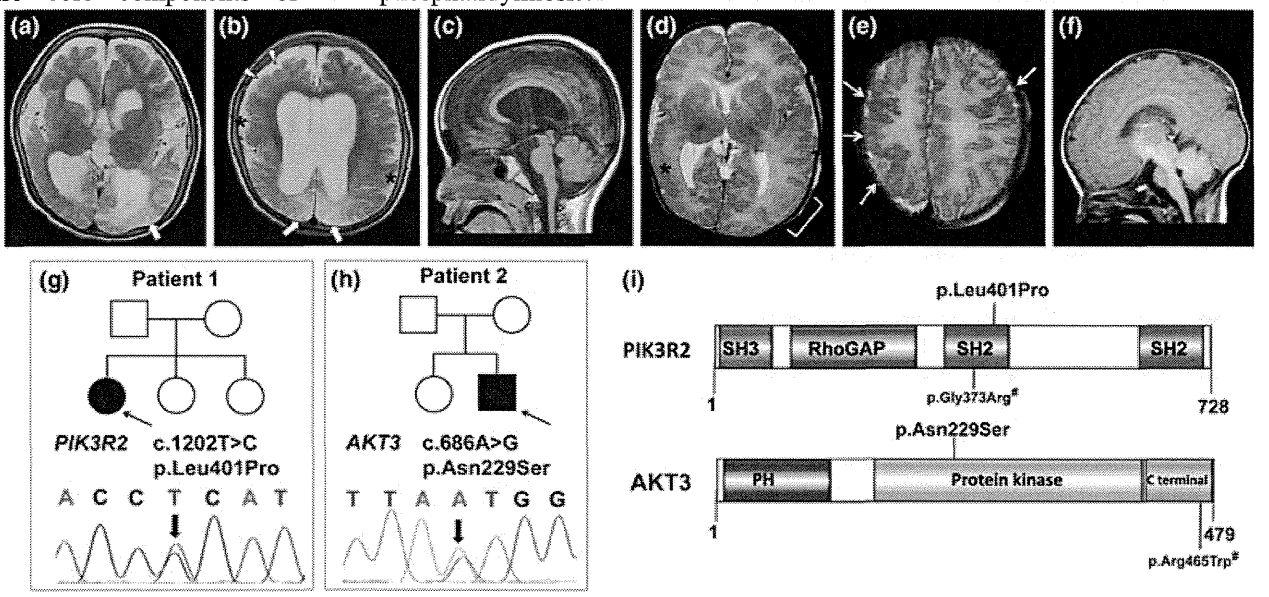

Fig. 1. Magnetic resonance imaging of patient 1 at 6 years of age (**a–c**). (**a, b**) Axial T2-weighted imaging showing enlarged lateral and third ventricles, enlarged extra-axial space, and decreased white matter volume with occipital lobe predominance. Irregular small gyri with areas of cortical thickening compatible with polymicrogyria are observed prominently in the bilateral perisylvian regions (asterisks) and the right frontal lobes (white arrowheads). Abnormal high-intensity signals are seen in the bilateral occipital lobes (thick white arrows). (c) Sagittal T1-weighted imaging showing normal brainstem and cerebellum. Magnetic resonance imaging of patient 2 at 7 days of age (**d–f**). (**d**) Axial T2-weighted imaging at the level of the basal ganglia showing enlargement of the left hemisphere. Polymicrogyria is seen in the perisylvian fissures with right-side dominance, which extends to the right temporal lobe (asterisk). The left parietal cortex shows a blurred border between the gray matter and the white matter (bracket), suggesting dysplasia of cortical development. (**e**) Axial T2-weighted imaging showing polymicrogyria in the right parietal lobe adjacent to the central sulcus (white arrows). (**f**) Sagittal T1-weighted imaging showing a relatively small pontine base. Family pedigrees and causative mutations (**g–i**). (**g**) Patient 1 with MPPH showing a *de novo* heterozygous missense mutation in *PIK3R2* (c.1202T>C, p.Leu401Pro). (h) Patient 2 with MCAP showing a *de novo* missense heterozygous mutation in *AKT3* (c.686A>G, p.Asn229Ser). (i) Distribution of mutations in *PIK3R2* and *AKT3*. SH2, Src homology 2 domain; SH3, Src homology 3 domain; RhoGAP, Rho GTPase-activating protein domain; PH, pleckstrin homology domain. #Reported by Riviere et al. (2).

of the skin. Brain MRI at 7 days showed an asymmetric cerebral hemisphere with right-dominant perisylvian polymicrogyria (Fig. 1d–f), and at 2 months showed a thin corpus callosum and progressive hydrocephalus. These findings were compatible with MCAP.

Whole exome sequencing using DNA extracted from blood leukocytes revealed a *de novo* missense mutation in each patient: p.Leu401Pro in *PIK3R2* (patient 1) and p.Asn229Ser in *AKT3* (patient 2) (Fig. 1g–i). Both mutations were absent from the 6500 eomes sequenced by the National Heart, Lung, and Blood Institute exome project and our 144 in-house control exomes. The read count for mutant alleles possessing p.Leu401Pro in *PIK3R2* was 47.7% (84/176 reads), and that for p.Asn229Ser in *AKT3* was 52.2% (128/245 reads). Therefore, these mutations are likely germline rather than mosaic mutations.

The novel *PIK3R2* mutation (p.Leu401Pro) in patient 1 is within the first Src homology 2 (SH2) domain of the PIK3R2 protein; this domain binds to phosphotyrosine-containing motifs and regulates many aspects of cellular communication (5). Eleven MPPH families have been reported to have a recurrent *PIK3R2* mutation (p.Gly373Arg), which is also located in the first SH2 domain (2). The phenotypes of all 13 cases with the p.Gly373Arg mutation were similar to that of patient 1 (Table 1) (1, 2), implying that impaired function of the SH2 domain is important in the pathogenesis of MPPH. The *AKT3* mutation (p.Asn229Ser) detected in patient 2 with MCAP has been reported in a case of MPPH (2). Furthermore, another case with a different *AKT3* mutation (p.Arg465Trp) was diagnosed with overlapping features of MCAP and MPPH (Table 1). These findings support the notion that the two syndromes have a common genetic basis. Interestingly, somatic mosaicism of an *AKT3* mutation causes hemimegalencephaly, which is similar to MPPH or MCAP (6, 7). Mutation screening of *AKT3* should be considered for patients with MPPH or MCAP as well as those with hemimegalencephaly, for whom pathological tissue is available.

MCAP and MPPH are categorized as overgrowth syndromes, as are Cowden disease and Proteus syndrome that are caused by abnormal activation of the PI3K–AKT pathway, which participates in diverse cellular processes (3, 8). The PI3K–AKT pathway is linked to mammalian target of rapamycin (mTOR) (6), which is a specific molecule for targeted therapeutics (sirolimus or everolimus). Further investigation into potential treatments for overgrowth syndromes is essential.

In summary, we have described two patients with either an *AKT3* or a *PIK3R2* mutation. Our data highlight the importance of the SH2 domain of PIK3R2 in MPPH, and support that MPPH and MCAP have the same genetic origin.

Table 1. Phenotypes associated with *PIK3R2* and *AKT3* mutations

Patient (diagnosis)	Patient 1 (MPPH)	13 patients[a] (MPPH)	Patient 2 (MCAP)	LR11-354[a] (MPPH)	LR08-018[a] (overlapping MCAP and MPPH)
Mutation	*PIK3R2* (p.Leu401Pro)	*PIK3R2* (p.Gly373Arg)	*AKT3* (p.Asn229Ser)	*AKT3* (p.Asn229Ser)	*AKT3* (p.Arg465Trp)
Features					
HC SD (age)	+2.6 (1 y 9 m)	+2–8 (8 m–13 y)	+3.0 (2 m)	+6.0 (2 y 5 m)	+5.5 (7.5 m)
Overgrowth	–	2/13	–	–	–
Vascular abnormalities	–	0/13	Skin capillary malformation	–	umbilical hemangioma
Connective tissue dysplasia	–	0/13	+	+	+
Syndactyly	–	0/13	–	–	–
Polydactyly	+	2/13	–	–	–
Epileptic seizures	+	6/9	+	ND	+
Visual impairment	+	ND	–	ND	ND
Neuroimaging features					
Polymicrogyria	+	13/13	+	+	+
Hydrocephalus or ventriculomegaly	+	13/13	+	+	+
CBTE	–	8/13	–	–	+

MPPH, megalencephaly-polymicrogyria-polydactyly-hydrocephalus syndrome; MCAP, megalencephaly-capillary malformation syndrome; HC, head circumference; SD, standard deviation; y, years; m, months; ND, no data; CBTE, cerebellar tonsillar ectopia.
[a] Rivière et al. (2) and Mirzaa et al. (1).

Acknowledgements

We would like to thank the patients and their families for their participation in this study. We thank Aya Narita for technical

assistance. This work was supported by the Ministry of Health, Labour, and Welfare of Japan (24133701,11103577, 11103340 and 10103235); a Grant-in-Aid for Scientific Research (C) from the Japan Society for the Promotion of Science (24591500); a Grant-in-Aid for Young Scientists from the Japan Society for the Promotion of Science (10013428 and 12020465); the Takeda Science Foundation; the Japan Science and Technology Agency; the Strategic Research Program for Brain Sciences (11105137); and a Grant-in-Aid for Scientific Research on Innovative Areas (Transcription Cycle) from the Ministry of Education, Culture, Sports, Science, and Technology of Japan (12024421).

K Nakamura[a,b]
M Kato[b]
J Tohyama[c]
T Shiohama[d]
K Hayasaka[b]
K Nishiyama[a]
H Kodera[a]
M Nakashima[a]
Y Tsurusaki[a]
N Miyake[a]
N Matsumoto[a]
H Saitsu[a]
[a]Department of Human Genetics
Yokohama City University Graduate School of Medicine
Yokohama, Japan
[b]Department of Pediatrics
Yamagata University Faculty of Medicine
Yamagata, Japan
[c]Department of Pediatrics
Epilepsy Center, Nishi-Niigata Chuo National Hospital
Niigata, Japan
[d]Department of Pediatrics
Kimitsu Chuo Hospital
Chiba, Japan

References

1. Mirzaa GM, Conway RL, Gripp KW et al. Megalencephaly-capillary malformation (MCAP) and megalencephaly-polydactyly-poly microgyria-hydrocephalus (MPPH) syndromes: two closely related disorders of brain overgrowth and abnormal brain and body morphogenesis. Am J Med Genet A 2012: 158A: 269–291.
2. Riviere JB, Mirzaa GM, O'Roak BJ et al. De novo germline and postzygotic mutations in *AKT3*, *PIK3R2* and *PIK3CA* cause a spectrum of related megalencephaly syndromes. Nat Genet 2012: 44: 934–940.
3. Franke TF. PI3K/Akt: getting it right matters. Oncogene 2008: 27: 6473–6488.
4. Tohyama J, Akasaka N, Saito N, Yoshimura J, Nishiyama K, Kato M. Megalencephaly and polymicrogyria with polydactyly syndrome. Pediatr Neurol 2007: 37: 148–151.
5. Liu BA, Jablonowski K, Raina M, Arcé M, Pawson T, Nash PD. The human and mouse complement of SH2 domain proteins – establishing the boundaries of phosphotyrosine signaling. Mol Cell 2006: 22: 851–868.
6. Lee JH, Huynh M, Silhavy JL et al. De novo somatic mutations in components of the PI3K-AKT3-mTOR pathway cause hemimegalencephaly. Nat Genet 2012: 44: 941–945.
7. Poduri A, Evrony GD, Cai X et al. Somatic activation of AKT3 causes hemispheric developmental brain malformations. Neuron 2012: 74: 41–48.
8. Lindhurst MJ, Sapp JC, Teer JK et al. A mosaic activating mutation in *AKT1* associated with the Proteus syndrome. N Engl J Med 2011: 365: 611–619.

Correspondence:
Dr Kazuyuki Nakamura, MD
Department of Pediatrics
Yamagata University Faculty of Medicine
2-2-2 Iida-nishi
Yamagata 990-9585
Japan
Tel: +81-23-628-5329
Fax: +81-23-628-5331
e-mail: kazun-yamagata@umin.ac.jp

BRIEF COMMUNICATION

Is focal cortical dysplasia sporadic? Family evidence for genetic susceptibility

*†‡[1]Richard J. Leventer, §¶[1]Floor E. Jansen, **††Simone A. Mandelstam, ‡‡Alice Ho, §§Ismail Mohamed, ¶¶Harvey B. Sarnat, ##Mitsuhiro Kato, ***Tatsuya Fukasawa, †††Hirotomo Saitsu, †††Naomichi Matsumoto, ‡‡‡Masayuki Itoh, §§§¶¶¶Renate M. Kalnins, ‡###Chung W. Chow, *†‡A. Simon Harvey, ¶**Graeme D. Jackson, ****Peter B. Crino, ¶Samuel F. Berkovic, and *‡¶**Ingrid E. Scheffer

Epilepsia, 55(3):e22–e26, 2014
doi: 10.1111/epi.12533

Dr Richard Leventer is a consultant pediatric neurologist at the Royal Children's Hospital.

Summary

Focal cortical dysplasia is a common cortical malformation and an important cause of epilepsy. There is evidence for shared molecular mechanisms underlying cortical dysplasia, ganglioglioma, hemimegalencephaly, and dysembryoplastic neuroepithelial tumor. However, there are no familial reports of typical cortical dysplasia or co-occurrence of cortical dysplasia and related lesions within the same pedigree. We report the clinical, imaging, and histologic features of six pedigrees with familial cortical dysplasia and related lesions. Twelve patients from six pedigrees were ascertained from pediatric and adult epilepsy centers, eleven of whom underwent epilepsy surgery. Pedigree data, clinical information, neuroimaging findings, and histopathologic features are presented. The families comprise brothers with focal cortical dysplasia, a male and his sister with focal cortical dysplasia, a female with focal cortical dysplasia and her brother with hemimegalencephaly, a female with focal cortical dysplasia and her female first cousin with ganglioglioma, a female with focal cortical dysplasia and her male cousin with dysembryoplastic neuroepithelial tumor, and a female and her nephew with focal cortical dysplasia. This series shows that focal cortical dysplasia can be familial and provides clinical evidence suggesting that cortical dysplasia, hemimegalencephaly, ganglioglioma, and dysembryoplastic neuroepithelial tumors may share common genetic determinants.

KEY WORDS: **Familial, Cortical dysplasia, Ganglioglioma, Hemimegalencephaly, Dysembryoplastic neuroepithelial tumor.**

Accepted December 2, 2013; Early View publication Feburary 6, 2014.

*Department of Neurology, Royal Children's Hospital, Melbourne, Victoria, Australia; †Murdoch Childrens Research Institute, Melbourne, Victoria, Australia; ‡Department of Pediatrics, University of Melbourne, Melbourne, Victoria, Australia; §Department of Pediatric Neurology, Rudolf Magnus Institute of Neurosciences, University Medical Center Utrecht, Utrecht, The Netherlands; ¶Epilepsy Research Centre, University of Melbourne, Austin Health, Melbourne, Victoria, Australia; **The Florey Institute of Neuroscience and Mental Health, Melbourne, Victoria, Australia; ††Department of Radiology, University of Melbourne, Melbourne, Victoria, Australia; ‡‡Departments of Pediatrics and Clinical Neurosciences, Alberta Children's Hospital, University of Calgary, Calgary, Alberta, Canada; §§Department of Pediatrics, IWK Health Center, Dalhousie University, Halifax, Nova Scotia, Canada; ¶¶Department of Pediatrics, Pathology, (Neuropathology) and Clinical Neurosciences, University of Calgary Faculty of Medicine, Alberta Children's Hospital, Calgary, Alberta, Canada; ##Department of Pediatrics, Yamagata University Faculty of Medicine, Yamagata, Japan; ***Department of Pediatrics, Anjo Kosei Hospital, Aichi, Japan; †††Department of Human Genetics, Yokohama City University Graduate School of Medicine, Yokohama, Japan; ‡‡‡Department of Mental Retardation and Birth Defect Research, National Institute of Neuroscience, National Center of Neurology and Psychiatry, Tokyo, Japan; §§§Department of Anatomical Pathology, Austin Hospital, Melbourne, Victoria, Australia; ¶¶¶Department of Pathology, University of Melbourne, Melbourne, Victoria, Australia; ###Department of Anatomical Pathology, Royal Children's Hospital, Melbourne, Victoria, Australia; and ****Shriners Hospitals Pediatric Research Center, Temple University, Philadelphia, Pennsylvania, U.S.A.

Address correspondence to Richard J. Leventer, Department of Neurology, Royal Children's Hospital, Flemington Road, Parkville, Vic. 3052, Australia. E-mail: richard.leventer@rch.org.au

[1]These authors contributed equally to this work.

Focal cortical dysplasia (FCD) encompasses a spectrum of cortical abnormalities characterized by dyslamination with or without abnormal cell types. FCDs are among the most common malformations of cortical development (MCDs) and are frequently associated with intractable epilepsy. FCD is often the only congenital abnormality present in the brain or elsewhere, with seizures usually being the sole clinical manifestation. The classification of FCD is based on the presence or absence of features in addition to cortical dyslamination: type I (no abnormal cell types), type II (dysmorphic neurons with or without balloon cells), and type III (type I with another lesion).[1] FCD may accompany hippocampal sclerosis and the "developmental" glioneuronal tumors, ganglioglioma and dysembryoplastic neuroepithelial tumors (DNETs), refining the classification to type IIIa and type IIIb, respectively.[1] A broad developmental classification of MCDs classifies the tubers of tuberous sclerosis complex (TSC), FCD type II, ganglioglioma, hemimegalencephaly, and DNET as all being malformations due to abnormal neuronal and glial proliferation with abnormal cell types.[2]

The etiology of FCD is largely unknown. Although the lesions of FCD (particularly FCD type II) share many imaging and histologic features with cortical tubers of TSC, FCD is usually sporadic, without clinical evidence to support a simple genetic etiology. Mutations in *CNTNAP2* have been reported in children with FCD from Old Order Amish pedigrees.[3] These children differed from most patients with FCD because of mental retardation and macrocephaly, and the imaging findings and histology were not typical of either FCD type I or FCD type II. There have been no other reports of familial FCD. Apart from a single report of a father-son pair with DNET,[4] clinical evidence is lacking to suggest a familial basis for ganglioglioma, DNET, or nonsyndromic hemimegalencephaly, or familial co-occurrence of FCD with hemimegalencephaly, ganglioglioma, or DNET. A role for human papilloma virus (HPV)16 infection in the etiology of FCD type IIb has recently been suggested from studies of resected tissue and a mouse model.[5]

Recent studies of resected tissue from patients with hemimegalencephaly identified de novo somatic mosaic mutations in the genes of the PI3K-AKT3-mTOR (mammalian target of rapamycin) pathway in 9 of 28 patients.[6,7] Evidence from molecular analysis of FCD specimens has led to the hypothesis that these malformations may have a shared pathogenesis, due to abnormalities of mTOR or other cellular pathways that regulate neuronal and glial proliferation.[8] However, until now, there has been no evidence to suggest a link between these disorders from family studies. Here, we report six families, each with two individuals with FCD, ganglioglioma, hemimegalencephaly, or DNET, adding clinical evidence that suggests a shared genetic susceptibility underlying these disorders, and showing for the first time that typical FCD can be familial.

Methods

Families were ascertained by referral to pediatric and adult epilepsy services. Clinical details were obtained from patient interview and medical records. Each institution's human research ethics committee approved the study. Informed consent was obtained from patients or their parents in the case of minors.

Brain magnetic resonance imaging (MRI) was obtained using age-specific epilepsy protocols on 1.5 T or 3 T scanners. Neurologists and neuroradiologists skilled in the detection of MCDs reviewed the MRI scans. Resected tissue was classified by a neuropathologist, according to the proposed system of the International League Against Epilepsy (ILAE) Diagnostic Methods Commission.[1] *TSC1* and *TSC2* mutation screening was performed using DNA extracted from resected brain tissue or whole blood using polymerase chain reaction (PCR) with exon-specific primers for *TSC1* and *TSC2* or by whole exome sequencing techniques.

Results

Six families, each with two affected individuals with seizures and at least one having FCD, were ascertained (pedigrees and selected MRI and neuropathology images: Fig. 1, clinical and imaging details: Table 1, additional MRI and neuropathology images: Fig. S1). All but one patient has undergone epilepsy surgery. None of the patients had clinical features suggestive of TSC, and all patients except family 5 were screened for *TSC1* and *TSC2* mutations. No mutations were identified.

Family 1 comprises brothers with neonatal seizures secondary to right hemisphere FCD type IIa, multifocal in patient 1A and restricted to the right posterior quadrant in patient 1B. The father and paternal uncle of these brothers have each had rare nocturnal seizures without focal features on interictal electroencephalography (EEG). Review of their recent brain MRI studies performed at 3 T revealed no abnormalities. Family 2 includes female 2A with FCD type Ia at the depth of an abnormal branch of the left central sulcus. Her female first cousin 2B had a ganglioglioma in the left superior temporal gyrus. Family 3 includes a female 3A with FCD type IIb in the right anterior temporal pole. Her male cousin 3B had a left middle frontal gyrus DNET. Family 4 includes female 4A with right occipital lobe FCD type IIb. Her nephew 4B had well-controlled focal seizures with a left posterior parietal region lesion on MRI, highly suggestive of FCD that was not removed (see Fig. S1). Family 5 includes a male 5A with an area of FCD type IIb at the depth of an abnormally deep left medial frontal lobe sulcus. His sister 5B had left temporal lobe imaging consistent with both hippocampal sclerosis and FCD in the posteromedial left temporal region, with cortical thickening, blurring of the gray-white

Epilepsia, 55(3):e22–e26, 2014
doi: 10.1111/epi.12533

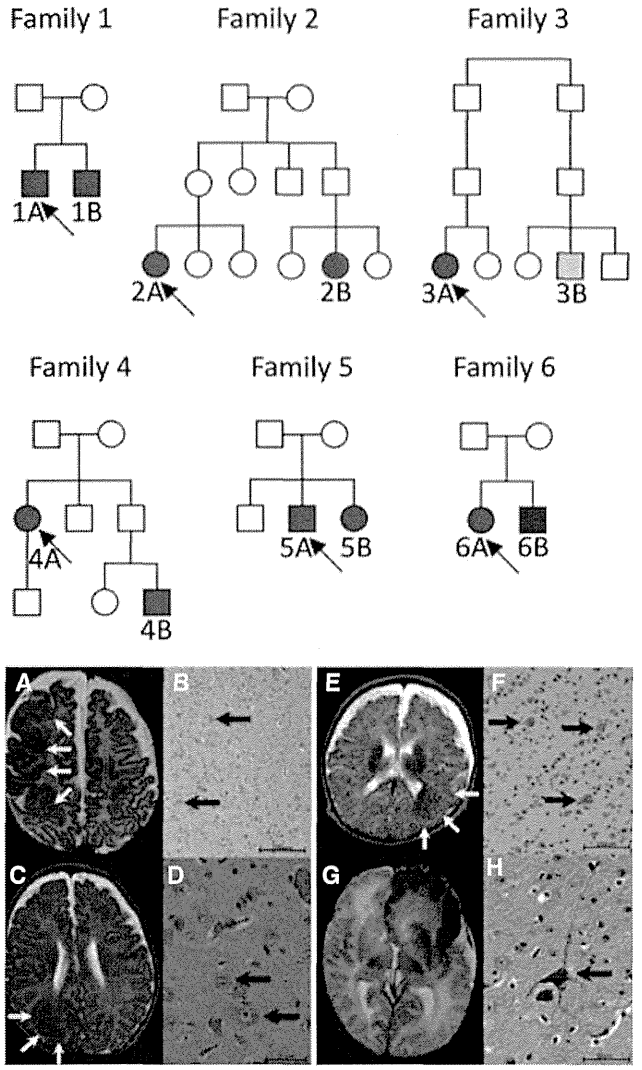

Figure 1.
Pedigrees of the six families and selected brain MRI and neuropathology images of families 1 and 6. **(A)** (top): The proband is marked with an arrow and is assigned "A" and their affected relative is assigned "B." Blue, focal cortical dysplasia; green, ganglioglioma; yellow, DNET; red, hemimegalencephaly. **(B)** (bottom): All MR images are T_2 axial and all pathology images are stained with hematoxylin and eosin (H&E). Family 1 is on the left panel and family 6 is on the right panel. MRI of patient 1A aged 6 weeks (**A**) shows multifocal areas of irregular and thickened cortex, irregular sulcation, and abnormal subcortical signal in the right hemisphere (arrows). MRI of patient 1B aged 14 weeks (**C**) shows an extensive area of irregular and thickened cortex with abnormal signal in the right posterior quadrant (arrows). Histopathology of both patient 1A (**B**) and patient 1B (**D**) showed cortical dyslamination with dense clusters of large dysmorphic neurons (arrows), irregular in orientation, often with prominent Nissl substance and bundles of pinkish fibrillary material in the cytoplasm. Balloon cells were not seen, consistent with FCD type IIa. MRI of patient 6A aged 8 weeks (**E**) shows loss of gray–white matter differentiation, abnormal sulcation, and low signal in the underlying white matter in the posterior left hemisphere (arrows). MRI of patient 6B aged 2 weeks (**G**) shows an enlarged left hemisphere with abnormal sulcation, poor gray–white matter differentiation, and abnormal signal throughout, most prominent in the frontal lobe suggestive of hemimegalencephaly. Histopathology from patient 6A (**F**) showed severe dyslamination and occasional dysmorphic neurons (arrows) consistent with FCD type IIa. Histopathology from patient 6B (**H**) showed abnormal lamination and dysmorphic neurons (arrow) with heterotopic neurons and microcalcification in the white matter. Balloon cells were not seen, consistent with FCD type IIa (within hemimegalencephaly).
Epilepsia © ILAE

matter junction, and high signal on T_2 and fluid-attenuated inversion recovery (FLAIR) images. Histopathology showed hippocampal sclerosis. It was not surprising that no histologic features of FCD were found as there was limited surgical tissue obtained from the abnormal posterior region. Family 6 includes a female 6A with a large area of FCD type IIa in the left posterior quadrant. Her brother 6B had left hemimegalencephaly, containing areas of severe dyslamination and dysmorphic neurons as seen in FCD type IIa.

Discussion

Despite its prevalence, and histopathologic similarity to the tubers in TSC, the molecular causes of FCD remain unknown, and there are no familial cases of typical FCD reported. This suggests that either FCD does not have a genetic basis, or that it does have a genetic basis but occurs sporadically, possibly due to somatic mutations in affected tissue. Evidence to support a relationship between FCD, DNET, hemimegalencephaly, and ganglioglioma has come from a number of sources. First, there are numerous reports of both FCD type I and FCD type II occurring with DNET and ganglioglioma,[9,10] and a report of DNET, ganglioglioma, and FCD coexisting in a "composite lesion" in one patient.[11] Second, an association of FCD, hemimegalencephaly, and ganglioglioma has been suggested from molecular and genetic studies of surgical specimens. These studies show that cytomegaly, seen not only in tubers of TSC but also in hemimegalencephaly, FCD, and ganglioglioma, may reflect aberrant activation of the mTOR and β-catenin signaling cascades, known regulators of cell growth, consequently causing defective control of neuronal and glial proliferation.[12–14] As found in our series, attempts to detect germ line or somatic mutations in *TSC1* and *TSC2* in patients with FCD and related lesions have largely been unsuccessful,[15] suggesting that abnormalities in other genes in the mTOR cascade or related pathways of neuronal proliferation and differentiation may play a role. If we assume that some forms of FCD, DNET, hemimegalencephaly, and ganglioglioma may have a shared etiologic mechanism and timing, then it is reasonable to consider that the occurrence of these lesions in closely related family members may be

Table 1. Clinical data for the six families

Patient	Age	Sz onset	Sz types	Ictal onset	Lesion localization	Age at surgery	Type of surgery	Pathology	Current AEDs	Outcome
1A	16 year	1 d	Tonic, L focal motor	Multifocal R hemisphere	Multifocal R hemisphere	6 m	Hemispherectomy	FCDIIa	NIL	Sz – free
1B	10 y	2 w	L focal motor	R posterior quadrant	R posterior quadrant	10 w and 5 m	Corticectomy + temporo-parietooccipital resection	FCDIIa	NIL	Sz – free
2A	37 y	7 y	R focal motor	L central	L precentral gyrus	27 y	L central corticectomy	FCDIa	LEV	>50% Sz reduction
2B	23 y	8 y	Focal dyscognitive with dysphasia	L temporal	L superior temporal gyrus	14 y	Lesionectomy	GG	NIL	Sz – free
3A	24 y	9 y	Focal dyscognitive with L arm dystonia	R anterior quadrant	R anterior temporal pole	14 y	Lesionectomy	FCDIIb	NIL	Sz – free
3B	28 y	12 y	Aphasia, R facial sensorimotor with generalization	L frontal	L middle frontal gyrus	17 y	Partial lesionectomy	DNET	LEV	>50% Sz reduction
4A	35 y	6 y	Visual aura then L arm dystonia with generalization	R occipital	R occipital	24 y	Lesionectomy	FCDIIb	NIL	Sz – free
4B	12 y	3 y	Focal dyscognitive with vomiting	ND	L posterior parietal	ND	ND	–	VPA	Sz – free
5A	14 y	3 y	Arousal and bipedal hyperkinetic movements	L frontal	L medial superior frontal gyrus	12 y	Lesionectomy	FCDIIb	CBZ, VPA	Sz – free
5B	12 y	4 y	Focal dyscognitive with bilateral hand automatisms +/– generalization	L temporooccipital	L hippocampus and parahippocampal gyrus	5 y	Lesionectomy and anterior temporal lobectomy	HS	CBZ	Sz – free
6A	5 y	1 m	Epileptic spasms and focal motor	L parietal	L posterior quadrant	8 m and 5 y	Focal corticectomy then L posterior quadrantectomy	FCDIIa	LTG, CBZ, PHT	Ongoing Sz
6B	4 m	1 d	Epileptic spasms and multifocal clonic	L frontal	R hemisphere	2 m	Functional hemispherectomy	FCDIIa (HME)	PHT, ZNS	Sz – free

ND, not done; VPA, sodium valproate; LEV, levetiracetam; LTG, lamotrigine; CBZ, carbamazepine; PHT, phenytoin; ZNS, zonisamide; FCD, focal cortical dysplasia; GG, ganglioglioma; DNET, dysembryoplastic neuroepithelial tumor; HME, hemimegalencephaly; HS, hippocampal sclerosis; Sz, seizure; y, year; m, months; L, left; R, right; d, days, w, weeks.

Epilepsia, 55(3):e22–e26, 2014
doi: 10.1111/epi.12533